Air–Sea Momentum Transfer by Means of Short-Crested Wavelets*

G. T. CSANADY

Woods Hole Oceanographic Institution, Woods Hole, MA 02543

(Manuscript received 20 November 1984, in final form 23 May 1985)

ABSTRACT

Recent laboratory studies of Okuda and others revealed shear stress "spikes" over wavelet crests as the principal instruments of air–sea momentum transfer. Examination of other laboratory evidence shows that sharp local intensification of skin friction is a characteristic of reattaching flow in *three-dimensional* separation only.

Flow reattachment over a downwind wavelet crest ensures the coincidence of high shear stress and downwind orbital velocity, resulting in energy input to the fluctuating motion, i.e., a coupling of the wavelets to the wind. Such coupling is shown to occur over short-crested wavelets at a specific waveheight-to-wavelength ratio.

Under the shear stress spikes a thin vertical layer develops on the water surface, which rides over the essentially irrotational motion of the wavelets. Thickening of the vortical layer over the windward face of a wavelet causes a positive pressure perturbation in quadrature with downward vertical velocity, which tends to transfer energy to the wavelet. A counter-effect occurs, however, because the surface velocity exceeds the phase velocity: vortical fluid accumulates ahead of the wave crest and exerts pressure where the vertical velocity is upward, extracting energy from the wavelet. When the two effects balance, on the average, the wavelets are in statistical equilibrium with the energy supply and their average amplitude remains unchanged.

Such equilibrium conditions can be maintained only for wavelets of a specific wavelength. This is shown by an argument relating to energy dissipation: with the wavelets in statistical equilibrium, the energy supply to the surface must be dissipated by the eddies of the turbulent surface shear layer. Standard hypotheses on turbulence lead to the result that the celerity of the wavelets coupled to the wind must be a function of the friction velocity.

Certain implications of the wind–wavelet coupling mechanism (inferred from laboratory evidence) for the aerodynamic roughness of the sea surface, and for the near-surface properties of the turbulent shear layer in water, are in satisfactory agreement with field evidence, suggesting that the same coupling mechanism also operates on a natural windblown surface.

1. Introduction

After many years of air–sea boundary layer research the precise mechanism by which wind stress is communicated to a water surface remains a puzzle. One important practical consequence is uncertainty affecting the calibration of a novel wind stress measuring instrument, the scatterometer: how should one expect the backscattered signal to depend on such material properties as viscosity or surface tension, and how should one best obtain a universally valid calibration algorithm for this instrument? The large amount of empirical information available on wind stress over water leads one to suspect that most of the relevant facts are known: lacking is the understanding necessary for organizing them into a coherent intellectual framework.

It has been known for some time that the sea surface is aerodynamically rough (e.g., see Roll, 1965). The usual explanation of the increased drag of a rough surface compared to a smooth one is that form drag (resultant pressure force) on the roughness elements, presumably due to flow separation, transfers most of the momentum. This has never been established empirically for rough solid surfaces, let alone a water surface. The empirical evidence merely shows that the drag increases when the roughness elements pierce the viscous sublayer, and that the drag is a function of the roughness Reynolds number for geometrically similar roughness. Different roughness patterns, however, cause different drag, and the reasons for this have not been explored, in spite of the hope expressed many years ago by Clauser (1956).

For a water surface, the conventional assumption that aerodynamic roughness implies the dominance of form drag leads to the conclusion that the momentum transferred to the water appears in the first instance as wave momentum (Stewart, 1961, 1974). As many investigators have concluded, the waves involved are short and steep. It is generally assumed that the momentum such wavelets acquire by means of form drag is transferred to the underlying shear flow and longer waves as the wavelets break (Longuet-Higgins, 1969a). Even if this scenario were to be verified, it would leave open the question of the wavelets involved in momentum transfer: what is their wavelength and amplitude, and what physical factors influence them?

* Woods Hole Oceanographic Institution Contribution No. 5721.

Much light has been thrown on this problem by recent laboratory investigations, notably those of Toba *et al.* (1975), Okuda *et al.* (1976, 1977), Kawai (1979, 1981, 1982), and Okuda (1982a–c). Laboratory wind–wave tanks are eminently suitable for the study of the interaction between air flow and underlying *short* waves, both mechanically generated and wind-induced, although of course they do not address the influence of the much longer and larger main wind waves of a natural water surface on the behavior of the short waves. One key laboratory discovery, made by Okuda *et al.* (1976, 1977), is that the force of the wind is transmitted predominantly not by form drag, but by sharp local amplification (a "spike") of the shear stress near, and just upwind of, the crests of short wind-waves. The physical properties of the wavelets responsible for the occurrence of the shear stress spikes have not been identified.

While there are clearly important differences between the short wind waves seen in a laboratory flume and the wavelets riding on a wavy sea, the possibility that momentum *may* be transferred principally by intermittent patches of high shear stress, rather than by form drag, opens up a new perspective in understanding air–sea momentum transfer. The difficulties raised by Ursell (1956) in regard to the weakness of the "sheltering" effect disappear when it is no longer necessary to attribute the increased shear stress of a rough surface to form drag. Ursell showed that, according to laboratory experiments on flow over a wavy surface, resultant pressure forces on roughness elements are about an order of magnitude too small to explain (long) wave generation by wind through Jeffreys's (1925) sheltering mechanism. His arguments also imply that form drag on short wavelets is insufficient to support the observed shear stress. If drag is supposed transmitted mainly by shear stress spikes, however, other difficult questions arise: by what mechanism can shear stress be amplified locally to well above its average value, and how can the multitude of wavelets, necessary for the transmission of the total wind stress force, be maintained?

A key insight comes from the consideration of the circumstances under which reattaching flow in the wake of a separation "bubble" will exert much greater than average shear stress on the underlying surface. Although experimental evidence on flow separation and reattachment behind wall-bound obstacles is not plentiful, what there is reveals clearly enough that shear stress amplification occurs only in three-dimensional separation. This is in accord with a suggestion made recently on the basis of qualitative visual observation (Csanady, 1984), to the effect that the principal roughness elements of a wind-blown sea surface are sharp- and short-crested wavelets, of 0.3 to 1 m wavelength, and a spanwise characteristic length of the same order. It is plausible to conclude that such wavelets cause air flow separation and that the reattaching flow generates shear stress spikes.

A third recent finding, supporting the above thesis, is that short-crested waves of "crescentic" shape arise spontaneously as a consequence of the hydrodynamic instability of finite amplitude wave motion. This important result has been established in a series of recent theoretical and experimental studies by Su *et al.* (1982), Su (1982), McLean (1982), Meiron *et al.* (1982), and others. The investigations apply to stagnant underlying fluid, so that it remains to be demonstrated that the same physical processes operate in essentially the same way if the underlying fluid is in long-wave motion. Nevertheless it is reasonable to suppose tentatively that the crescentic wavelets arise readily enough at an early stage of wave generation by wind. As discussed below, they are then coupled to the air flow through energy supply via the shear stress spikes.

The above tentative ideas are developed in greater detail below. Some implications of the shear-stress spike mechanism of momentum transfer are also explored. The question of long-wave/short-wave interaction is not addressed, so that the results are relevant in the first instance to water surfaces at short fetch, such as, for example, the surface of a lake. It is also shown, however, that field evidence on air–sea momentum transfer at *arbitrary* fetch is generally in accord with deductions from the wind–wavelet coupling mechanism.

2. Shear stress spikes and air flow separation

The air and water flow fields of a train of wavelets of specific celerity (phase velocity) c are simplest in a frame of reference moving with the wavelets. Figure 1 illustrates these fields schematically for a two-dimensional wave of moderate steepness, such that the surface velocity in an absolute frame nowhere exceeds the celerity c. In the moving frame the interface then has an upwind velocity everywhere. The air in contact with the water also moves upwind to a critical height z_c. Model calculations of the air flow above waves usually show closed streamline regions centered on the critical height ("cat's eyes"), see the dotted contour in Fig. 1

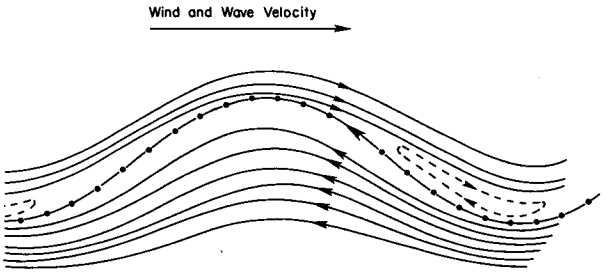

FIG. 1. Streamlines in a wave-following coordinate system for air and water, for a regular wave of moderate steepness and celerity much less than free stream wind speed. Free surface (dot-dashed) moves everywhere upwind, but the critical level is very close, the "cat's eye" (dashed) quite small.

(this was transposed from Fig. 8a of Gent and Taylor, 1977). It is important to note that for short wind-waves the celerity (c = 0.3 to 1.0 m s^{-1}) and the friction velocity in air u_{*a} in moderate to strong winds (U_a = 5 m s^{-1} and up) are of the same order of magnitude. The critical layer in such cases lies very close to the surface, and z_c is small compared to wave amplitude.

A fundamental point, usually taken for granted, is worth making explicitly here: the laws of motion are unaffected by the transformation of coordinates to the frame moving with the waves, including the laws that govern the behavior of boundary layers and turbulence. Thus boundary layer arguments can be used relating to the steady mean flow illustrated in Fig. 1: such arguments have, in effect, been tacitly relied upon by Gent and Taylor (1977), Hsu and Hsu (1983), and many earlier investigators.

The remarkable discovery of Okuda *et al.* on the distribution of shear stress over the surface of wind-wavelets (order 10 cm wavelength) is illustrated here in Fig. 2, reproduced from Okuda *et al.* (1977). This was inferred from the surface velocity gradient observed in the thin, laminar vortical layer riding on the surface. In the case shown here, the mean stress was 3 cm^2 s^{-2}, so that the highest four observed values average out to seven times the mean, occurring at −30° or so phase, i.e., just upstream of the crest. At phase >30° the stress becomes negligible. Although the measurements did not resolve the stress distribution near the wave crest on account of the chaotic nature of the water flow, Okuda *et al.* were able to show that the total shear force considerably exceeded the total form drag (the latter having been "at most several percent" of the total shear force).

Parallel investigations of the air flow above similar wavelets in the same wind tunnel by Kawai (1981, 1982) showed that the domain of vanishing shear stress ahead of the crest coincides with a region of separated air flow, the shear stress spike with the region of flow reattachment. Kawai's observations gave some indication of the streamline pattern in and around the separation region. Figure 3 here has been traced from Kawai's Fig. 12a with the streamlines drawn in to indicate flow direction (shown by little arrows in the original paper). The eddying motion is clearly complex, the separation region large. The magnitude of the flow velocity above the separation region rose to that of the free stream U_a within a millimeter or two. At U_a = 7 m s^{-1}, the air flow was found to separate from a large fraction (more than half) of the waves examined.

That the air flow separates from short wind-waves was pointed out a number of years ago by Schooley (1963). Detailed and quantitative studies of 27 cm wavelength wind-waves in a laboratory flume by Chang *et al.* (1971) also clearly showed air flow separation. This early experimental evidence on air flow separation was questioned, or at least reinterpreted, by Banner and Melville (1976) and Gent and Taylor (1977). Banner and Melville argue that the air flow can separate only if the interface velocity vanishes at some point,

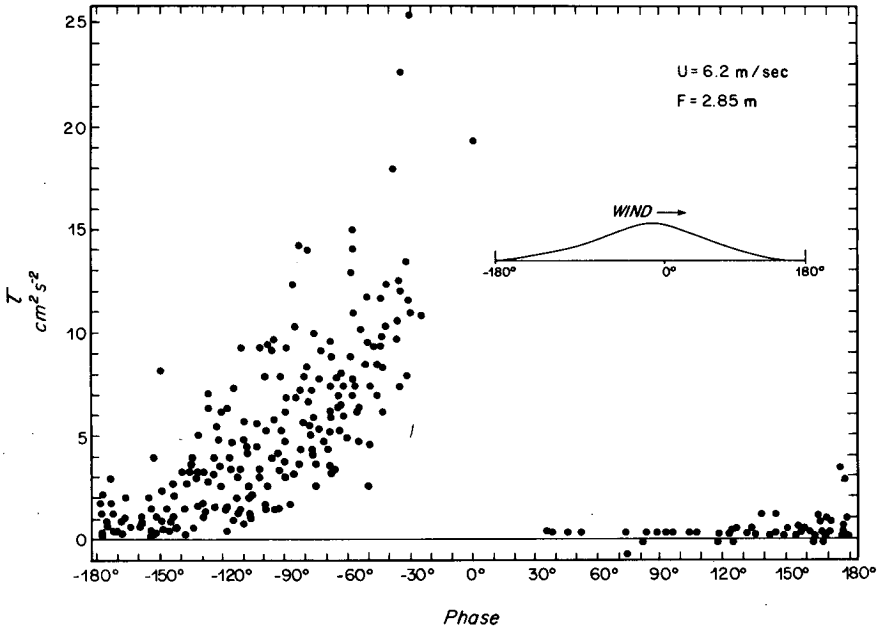

FIG. 2. Shear stress distribution along surface of wind wavelets, observed by Okuda *et al.* (1977). Although values right at the crest (−30° to +30° phase) could not be determined with certainty, circumstantial evidence showed the peak stress to be not much above the value observed near −30°. Area-mean stress was 3 cm^2 s^{-2}, so that the peak was of the order of five times the mean. On the leeward side the stress became vanishingly small.

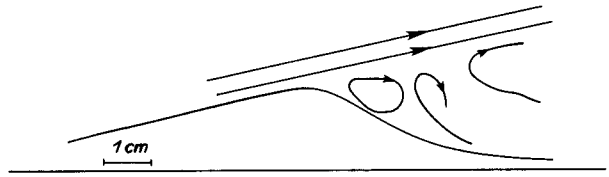

FIG. 3. Air-flow streamlines over a steep wind-wavelet of 11 cm wavelength, drawn approximately on the basis of the observations of Kawai (1982). The air speed above the separated flow region rapidly rises to the free-stream value: no attempt was made to show this by streamline spacing.

and that the separation streamline leaves the surface at such a common stagnation point of air and water flow. Gent and Taylor state that "the essential distinction to be made is between separation . . . and a thickening of the closed streamline region." These arguments apparently arise from a confusion of kinematic constraints with the dynamical phenomenon of flow separation, as the latter is understood in experimental fluid mechanics.

Kawai's observations leave no doubt about the *fact* of air flow separation over short wind-waves. There is no reason to doubt that the dynamical reason is the well known one: the onset of separation depends on the interplay between the adverse pressure gradient on the downwind side of a wave, and the turbulence in the air flow. To the extent that the small amount of boundary layer fluid (in air) below the critical level influences separation, it should cause separation to occur at a slightly smaller adverse pressure gradient than over a similar solid surface, and it should shift the separation point farther upwind, because of the counterflow of air and water. In other words, air flow over wavelets should be slightly more prone to separation than over a solid surface of the same geometry, but should not otherwise behave differently (at high U_a/c, when the air flow streamlines tend to follow the water surface closely).

The more important questions relating to the separating air flow are, how the skin friction can be amplified many times over its average value, and under what conditions the shear stress spike will coincide with a downwind wave crest. The latter question is relevant to the energy balance of the fluctuating motion (in water), because a shear stress maximum at the crest is in quadrature with the orbital velocity, and represents energy transfer across the interface.

3. Properties of the reattaching air flow

The reattachment of the separated air flow takes place downwind of the crest, at a distance that is presumably a sensitive function of wave shape. As Fig. 3 shows, the sharp-crested wavelets of interest in the present context have a nearly straight back (upwind) portion. Over a two-dimensional wave train, the flow following the straight back, separating at the crest and forming a bubble before reattaching before the next crest, would be similar to what one finds over and behind a "backward" facing step, see Fig. 4. This kind of flow was studied by a number of investigators, notably Bradshaw and Wong (1972) and Chandrsuda and Bradshaw (1981).

Bradshaw and Wong (1972) quote a number of experimental studies of flow separation and reattachment for two-dimensional obstacles of a shape similar to the typical wavelet illustrated in Fig. 3. The separation bubble length in all these cases was between 6 and 7 times the step height. Translating this to the geometry of a straight-back wavelet, and taking $ak = 0.33$ (a typical wave steepness in Kawai's observations) one calculates a separation bubble length of one and a half times the wavelength, or much too long for reattachment before the next wave crest. For irregular wind wavelets such a calculation is somewhat simplistic and merely suggests that something is wrong with the two-dimensional separation analogy.

More conclusive is the Reynolds stress distribution in two-dimensional separated flow behind a backward facing step, documented by Chandrsuda and Bradshaw (1981). The wall shear just downstream of the reattachment point rises rapidly and decays slowly afterwards. The maximum wall shear stress, however, is not very different from the shear stress on a flat plate. In contrast, the Reynolds stress a short distance above the wall, in the center of the high-shear region coming off the top of the separation bubble, is an order of magnitude greater. The measurements of Chandrsuda and Bradshaw extended to the terms of the shear-stress balance equation: these show that the principal generation term ($w^2\partial U/\partial z$) is relatively small near the wall, as one might expect from the vanishing of w and $\partial w/\partial z$. The shear stress is augmented there by turbulent transport from the center of the high shear region, but not enough to produce high wall shear. The large stress gradient between the wall and the high shear region is used to accelerate the low speed fluid within the separation bubble: in order to bring the velocity profile eventually close to that of an undisturbed boundary layer, such a

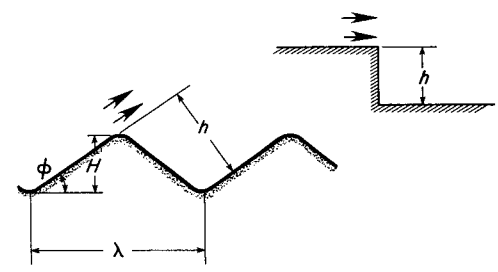

FIG. 4. Analogy between a backward facing step (top right) and sharp-crested wavelets. The effective step height h is approximately twice the waveheight, for small steepness ϕ, and a nearly symmetrical wave.

stress gradient must necessarily develop in two-dimensional flow.

The relatively smooth distribution of wall shear stress in two-dimensional flow behind a backward facing step is strikingly unlike that over Okuda's wavelets. Moreover, both the observed shortness of the separation region and the high shear stress upon reattachment suggest a three-dimensional separating flow pattern over wavelets.

Separation regions behind three-dimensional wall-mounted obstacles are generally shorter than in comparable two-dimensional flow, apparently for the reason that the low speed fluid behind the obstacle can also escape sideways. Castro and Robbins (1977), for example, show that the reattachment point in the wake of a floor-mounted cube of edge length h is located at a distance of about $2.7h$ behind the leading edge. This compares with $13.5h$ behind a two-dimensional gate of square cross-section (Bradshaw and Wong, 1972).

The pattern of separating and reattaching flow around three-dimensional wall-mounted obstacles is considerably more complex than over two-dimensional obstacles. Hunt *et al.* (1978) discuss the kinematics of this problem in some detail and show the streamline pattern in the center plane of a three-dimensional hump, redrawn here in a somewhat simplified form in Fig. 5. One major difference compared to a two-dimensional pattern is the occurrence of spiral nodal points N in this plane, towards which the flow spirals inward, to escape sideways in the third dimension. There is also a saddle point S of the streamlines above the surface. On the surface there are two separation points s and two reattachment points r. In plan view, i.e., over the surface of the obstacle, both separation points are saddle points, indicated by the separate little sketch, and both reattachment points are ordinary nodal points, from which the flow diverges (the different kinds of singular points are discussed by Lighthill, 1963).

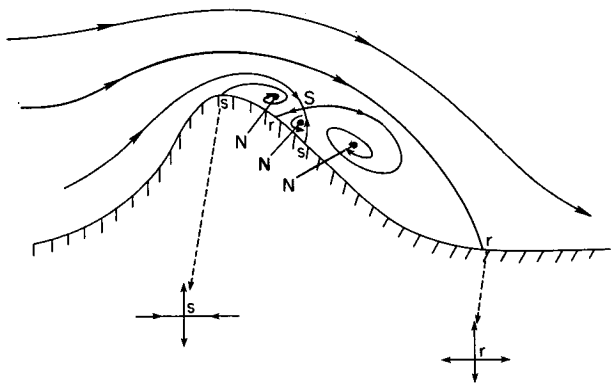

FIG. 5. Streamlines of separated flow in the center plane of a three-dimensional hump, redrawn from Hunt *et al.* (1978). Note various singularities, in particular spiral nodal points N, to which flow converges.

The most important departure from the two-dimensional flow pattern is that the streamline ending at the second (rear) reattachment point is not the one that separates at the first (front) separation point, but comes from the free stream. Thus the separation "bubble" is not a closed stream surface, but is in communication with outer streamlines, i.e., the fluid it contains escapes sideways to the trailing vortices, as already clear from the presence of the spiral nodal points N.

There is a degree of similarity between this flow pattern behind the hump of Hunt *et al.* (1978) and Kawai's observed velocity field over a wind–wavelet (Fig. 3): Kawai finds a small vortex just behind the top of the wavelet, and a second larger vortex farther downwind. Although the small reverse vortex (the center spiral nodal point N in Fig. 5) is not discernible from Kawai's figure, the kinematics of the streamlines requires its presence. Kawai further states that more complex vortex patterns can be observed, and that there is a great deal of variability in the behavior of the separated flow region. Hunt *et al.* point out that further complexities exist in the flow approaching the obstacle, and can arise from any asymmetry of the obstacle's shape. One more observation reported by Kawai is relevant, as he puts it: "The most prominent phenomenon observed in the present experiment is a blowing up of a low-speed air mass," over the crest and just over the windward face of a few waves. Although these events occur infrequently, they cause sharp Reynolds stress spikes in the air flow. Presumably, the low speed fluid in such bursts comes from low speed regions behind wavelets.

The differences between two- and three-dimensional separation regions are such as to bring high speed, free stream fluid closer to the surface following reattachment in the three-dimensional case. At least some of the separated fluid is allowed to escape sideways, removing a source of drag on the streamlines above. This provides the conditions under which a shear stress spike may be expected to develop on the surface.

The three-dimensional flow pattern near the reattachment point (near point r in Fig. 5) is divergent, with the vortex lines of the nearsurface shear flow being stretched. As Lighthill (1963) points out, this is the essential mechanism by which turbulence increases wall shear stress. Recent work on turbulent flow revealed the presence of large "horseshoe" eddies involved in the vortex stretching process, which give rise to the burst-sweep cycle of events near the wall (Laufer, 1975; Willmarth, 1975; Brown and Thomas, 1977; Thomas and Bull, 1983). A wall shear-stress spike accompanies this cycle in its sweep phase (e.g., see Thomas and Bull, 1983, their Fig. 21). The flow around a three-dimensional wall-mounted obstacle is similar to that of the horseshoe-vortex turbulence element, with the horseshoe turned closed end upstream instead of downstream. The effect on wall shear should be qualitatively the same: vortex lines are stretched and high speed fluid is brought close to the surface in the down-

draft (horizontally divergent) region. The shear-stress balance is similarly affected, and wall shear stress is increased on account of the sweeps of high speed fluid.

In the atmospheric boundary layer the sweep phase of such a cycle is perceived as a gust of wind, which, over a water surface, produces a cat's paw. The scale of the eddies involved is measured in tens to hundreds of meters. A similar phenomenon may well occur on a much smaller scale in the wake of short-crested wavelets, a kind of miniature cat's paw.

To sum up this discussion of air flow, the evidence suggests that the separation–reattachment process over wind-blown wavelets of the kind studied by Kawai and Okuda is three-dimensional, with at least some of the low speed fluid escaping sideways and up into the free stream, resulting in a shorter distance to the reattachment point than in two dimensions, and in strong local amplification of surface stress in the region of reattachment. By inference, the wavelets causing this kind of separated flow must be short crested. It should be noted here, however, that neither Kawai nor Okuda, in several very carefully written reports on their investigations, mention that the wavelets involved were short crested: they merely emphasize their irregularity. The laboratory flume they used was 15.3 cm wide, or barely enough to allow a recognizably crescentic shape to form. Nevertheless, for the purposes of further discussion it will be supposed that the wavelets transferring momentum from air to water at moderate to high wind speeds are short crested and thus able to generate shear stress spikes.

4. Selection of wave steepness

Under what condition will the air flow reattach somewhat upwind of the next wave crest? At the high Reynolds numbers in question the answer should lie entirely in the geometry of the wave field. Consider a vertical section parallel to the phase velocity across a train of short-crested wavelets of wavelength λ, Fig. 6. The spanwise location of the section is such that it cuts through the steepest part of some wavelets. Over these the air flow separates. The next downwind wavelet is not necessarily steep enough (owing to spanwise variation of amplitude) to cause separation in this location, but this is unimportant: if the length of the separation region b is about equal to three-quarters of a wavelength, the reattaching flow exerts its strongest drag near the next (perhaps not very steep) wave crest. The wave train may in this sense be thought directly coupled to the wind, provided that

$$b \approx \frac{3}{4}\lambda. \tag{1}$$

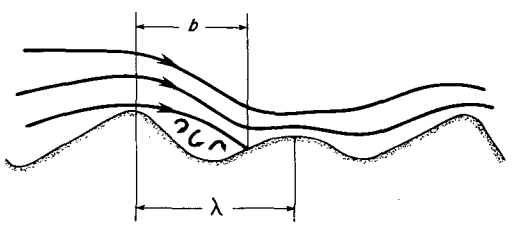

FIG. 6. Flow reattachment over the next downwind wavecrest.

For a given wave train, the length b of the separation region behind the steepest part of the wavelets should be a function of a characteristic wave height H, the downwind wavelength λ or wavenumber $k = 2\pi\lambda^{-1}$, and the cross-wind wavenumber l. Other geometric parameters, viscosity and capillarity are presumably of second order in importance. One has, therefore, approximately

$$\frac{b}{\lambda} \approx \text{func}\left(\frac{H}{\lambda}, \frac{l}{k}\right). \tag{2}$$

For crescentic wavelets arising from the instability of finite-amplitude wave motion the ratio l/k is of order one and may be expected to move within a narrow range. Setting $l/k \approx$ const, one concludes from the last two equations that also

$$\frac{H}{\lambda} \approx \text{const}. \tag{3}$$

One may think of this result as the outcome of a kind of natural selection mechanism. Coincidence of the shear-stress spikes with the next wave crest favors the survival of a wave train. The coincidence is brought about by the short-crested or crescentic character of the wavelets, which allows them to generate shear stress spikes, and by given steepness, which ensures the correct location of those spikes.

The hypothesis embodied in Eq. (1) may be tested by comparing its consequence, Eq. (3) with laboratory observations of Kawai (1982). Figure 7 shows Kawai's results on the steepness versus height of 79 wavelets examined (Kawai's Fig. 14). The open symbols denote waves with air flow separation. Their steepness clearly clusters around $H/\lambda = 0.08$ within a remarkably narrow range: practically all points fall within a range of $H/\lambda = 0.65$ to 0.95. Considering that only approximate equality is required in Eq. (1) for the selection mechanism to operate, the data support the hypothesis. Inverting and generalizing the argument, one may conclude that short-crested wavelets of a specific geometry become coupled to the wind by means of the shear-stress spike mechanism.

The reader will notice also that the points in Fig. 7 cluster around a linear relationship, implying $\lambda \approx$ const $= 12$ cm. In the Tohoku University studies, and in other wind–wave flume experiments, the wind-driven wavelets had a well defined dominant wavelength and celerity. This point will be discussed in a later section.

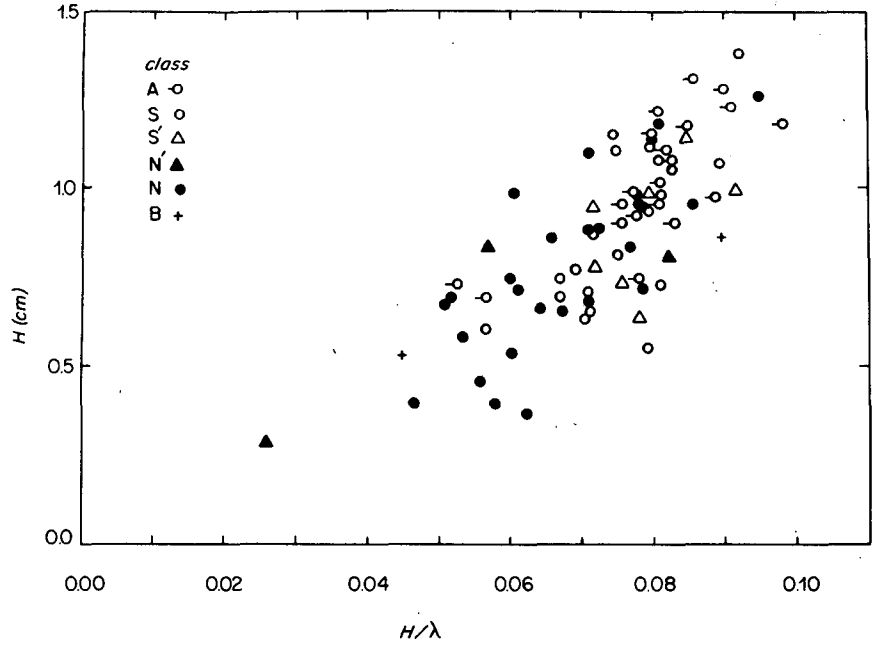

FIG. 7. Waveheight H versus waveheight-to-wavelength ratio H/λ of 79 wavelets analyzed by Kawai (1982). Open symbols refer to wavelets with certain or probable air flow separation, full symbols to other waves. Note narrow range of scatter around $H/\lambda = 0.08$, especially for wavelets with separating air flow.

5. Momentum transfer below the surface

The flow field in *water* under a natural wind-blown surface may be expected to consist of motions on several different scales: a thin surface boundary layer of high vorticity, nearly irrotational motion in short waves on top of longer waves, and an underlying turbulent shear flow in the free-surface shear layer. In his careful laboratory observations Okuda (1982a) was able to elucidate the details of the first two flow components, a high vorticity layer above a nearly irrotational, harmonic short wave. The high vorticity layer was generally thickest ahead of the crest, and stretched out on the windward side. Note that the windward side of the wave is *downstream* of the crest from the point of view of the water flow in a wave-following frame (cf. Fig. 1). The boundary layer is thinnest just downstream of the crest, thickening further away. Figure 8, from Okuda *et al.* (1977), illustrates this boundary layer growth, which is as envisaged by Longuet-Higgins (1969b) in his analysis of wave generation by fluctuating shear stress. The details of the velocity measurements have also demonstrated that a very thin surface slice of the high vorticity layer moves *upstream* from the windward side into an accumulation of low speed fluid just under and upstream of the crest (i.e., the surface moves faster with the wind than the wave, in a stationary frame). The low-speed fluid accumulation is transient and is occasionally ejected downward in a burst, although more usually it just drains away with the boundary layer fluid downstream, without causing a major disruption of the flow pattern. The wave height in these observations was typically 1 cm, the wave length 11 cm, and the maximum boundary layer thickness just under the crest 0.3 cm.

As already discussed, the drag force of the air was exerted mainly by a shear-stress spike downstream (i.e., upwind) of the wave crest. The momentum was thus transferred in the first place to the thin region of the high vorticity layer, from where some of it diffused *in situ* downward, while some of it was advected upstream into the low speed fluid accumulation. In the steeper waves a considerable momentum deficit was temporarily stored near the crest, to be either eventually drained away slowly, or released in an occasional burst.

The velocity distributions observed well away from the low-speed fluid accumulation can be readily resolved into a viscous boundary layer and an underlying irrotational wave motion. Figure 9, middle left, shows a velocity distribution in a wave trough (Okuda's Fig. 4, case III, profile 1), with the extrapolation of the wave-orbital velocity indicated. The velocity defect u_d of the viscous boundary layer is the difference between the extrapolated and the observed profiles.

Because the surface layer flow is disrupted at the crest by the low-speed fluid accumulation and reverse flow, the momentum deficit of the viscous boundary layer may be supposed to have been caused entirely by the stress spike downstream of the crest. Given that the absolute velocities $u - u_d$ (u: velocity of irrotational

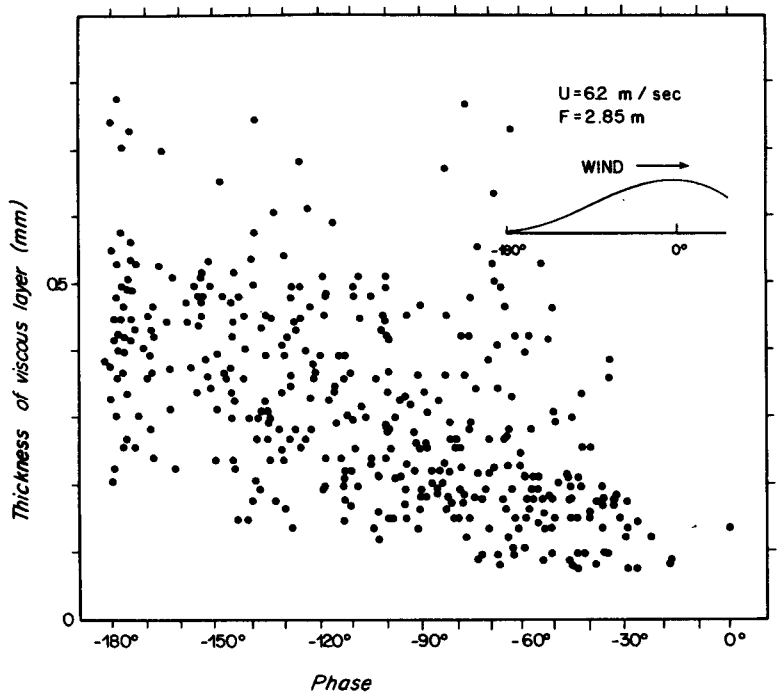

FIG. 8. Thickness of high-vorticity layer on the windward side of wavelets analyzed by Okuda *et al.* (1977). Note clear growth trend in the downstream direction of the water flow in the wave-following frame.

wave motion) at this section were small compared to the phase velocity c, the momentum integral relationship may be written approximately as:

$$c\int_{-\infty}^{0} u_a dz \approx \int_{0}^{x_c} \tau dx \equiv \tau_a \lambda \qquad (4)$$

where the integration of the shear stress extends to some point x_c near the crest, where a new viscous boundary layer begins to develop. The wavelength-average shear stress τ_a thus includes only that part of the shear stress spike acting over the thin portion of the high vorticity layer.

Even this partial stress impulse, calculated from the total momentum deficit as written down in Eq. (4), yields for the profile in Fig. 9 an average stress τ_a of 2 $cm^2\ s^{-2}$, twice the average wind stress over the whole water surface quoted by Okuda. The velocity profile in the next upstream trough (profile 8 in the same illustration of Okuda) gives a value of about $\tau_a = 0.5$ $cm^2\ s^{-2}$. Because some of the viscous layer drains upstream into the low-speed fluid accumulation, the momentum deficit of the viscous layer should in general be less than what corresponds to the area-average wind stress.

The viscous wake is disrupted by the next low-speed fluid accumulation and may be supposed to become part of a broader turbulent wake. The momentum deficit of the latter is distributed over a greater depth range and is not readily determined from Okuda's observations. Similar wakes have, however, been studied behind larger, isolated breaking waves in the laboratory by Peregrine and Svendsen (1979) and Battjes and Sakai (1981). The nose of a breaker contains a low-speed fluid accumulation much as a wind wave. The low speed fluid drains away in a trailing turbulent wake, as shown by the photographs of Peregrine and Svendsen, who made the wake visible by dye injection. A somewhat similar process may be thought to occur under wind wavelets, although the situation here is complicated by the further addition of momentum deficit at downstream wave crests. Another important difference is that the eddying motion receives energy directly from the wind, instead of being produced entirely by the shear flow as in the two-dimensional wake of a solid object.

6. Energy supply to the water surface

In spite of the considerable difficulty that attends measurement of surface velocity near the crest of short wind waves, Okuda (1982a) was also able to show that the surface velocity distribution along a wavelet was very uneven, similar to that of the shear stress. In the majority (85%) of wavelets observed (a total of 335) the peak surface velocity in a stationary frame was greater than the phase velocity, i.e., in a wave-following frame there was upstream flow in a thin surface layer. This resulted in a stress–velocity correlation $\overline{\tau' u_0'}$ large

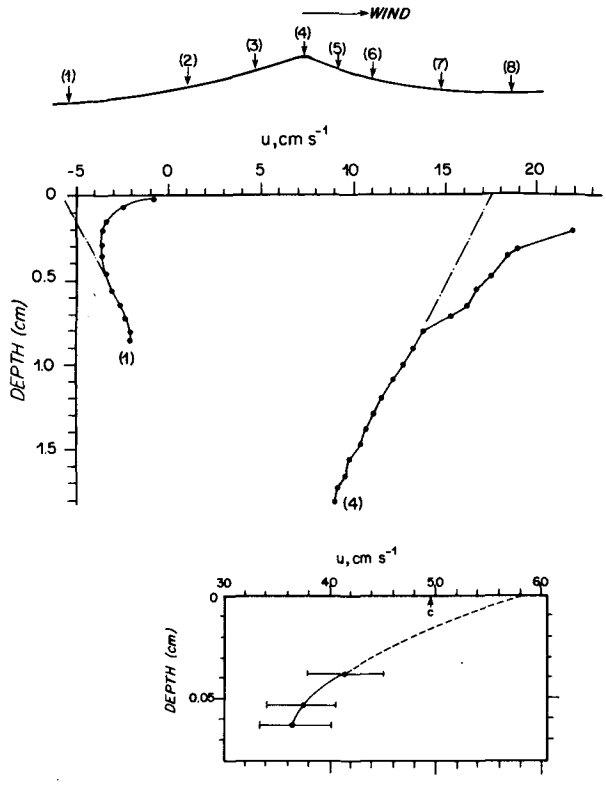

FIG. 9. Vertical distribution of velocity (in a stationary frame) in a steep wavelet observed by Okuda (1982a). Extrapolation to the surface (dot-dashed) shows orbital velocities of 12 cm s^{-1} superimposed on a mean flow of 6 cm s^{-1}. The separate small sketch shows near-surface details at the wave crest, observed in a similar wavelet by Okuda *et al.* (1977), with the phase velocity $c \approx 50$ cm s^{-1} indicated.

enough to be the dominant contribution to air–water energy flux. The total downward energy flux is the inner product of the stress tensor and the velocity at the interface. To a satisfactory approximation this is given by

$$F_0 = \tau U_0 + \overline{\tau' u_0'} + \overline{p' w_0'} \qquad (5)$$

where primes denote deviations from the area-average, overbars area-averages and the subscript zero surface values; τ is area-average stress, U area-average velocity, p is pressure, w vertical velocity.

In the cases analyzed by Okuda (1982a, c) the mean stress–velocity product τU_0 was approximately 12 cm^3 s^{-3}. For the stress–velocity correlation $\overline{\tau' u_0'}$ Okuda estimated a value of 20 cm^3 s^{-3}. This may have been an underestimate, because it was based on a stress–impulse over a wave equal to $\tau_a \cdot \lambda$ where τ_a is the area-average wind stress. As seen earlier, the laminar wake velocity defect on a steeper wavelet was twice the area average, so that the stress fluctuation was also about a factor of two higher on this wavelet. The exact numbers are not very important, only the fact that the stress–surface velocity correlation tends to be rather larger than the product of mean stress and mean surface velocity. The $\overline{p' w_0'}$ correlation was generally small, and in one of the four cases analyzed in detail *positive,* signifying upward (water to air) energy flux (this can be inferred from Fig. 3 of Okuda, 1982c, which shows surface pressures, and Fig. 4 of Okuda, 1982b, giving surface velocities).

It is tempting to interpret the terms on the right of Eq. (5) as energy supply to the mean shear flow and to the wavelets respectively. However, if the wavelets are essentially irrotational, their energy can only be increased by pressure forces acting in quadrature with the velocity, the $\overline{p' w_0'}$ term, which is small.

This difficulty can be resolved by a conceptual separation of the wave motion from a vortical layer riding on the surface, as in Longuet-Higgins's (1969) analysis of wave generation by fluctuating shear stress in a fluid of small viscosity. Longuet-Higgins showed that a viscous boundary layer develops on the surface over which a fluctuating stress acts, and that the boundary layer fluid is disposed on the surface in such a way that its weight provides the pressure forces necessary for energy transfer to the wavelets: the boundary layer thickens on the windward side, and presses down on the irrotational fluid below, at locations where the vertical velocity is downward. As was seen above, this effect did in fact occur over Okuda's wavelets.

Longuet-Higgins (1969b) assumed that the flow near the surface was laminar, and that the velocities in the boundary layer (in the wave-following frame) were everywhere in the same direction as the deeper irrotational motion. Neither of these approximations apply to the wavelets studied by Okuda, so that some differences in the disposition of the boundary layer fluid on the surface should be expected. Nevertheless, the general result of Longuet-Higgins's analysis, that the pressure distribution on the top streamline of irrotational motion differs significantly from that on the surface, remains useful in the interpretation of the observations.

Okuda (1982a) tested this idea by calculating the pressure distributions in question from the observation of the velocity field. He was able to show that the pressure distribution on the top streamline of the irrotational wave motion indeed differed substantially from the surface pressure distribution. Four wavelets were analyzed by Okuda in detail. On a wavelet with less than average slope the main departure from a smooth sinusoidal pressure distribution on the top streamline of the irrotational flow was a bulge over the windward side, in quadrature with downward velocity, as expected from the thickening of the shear layer downstream of the crest (in a wave-following frame) in accordance with Longuet-Higgins's theory. In the case of the steeper wavelets, however, although this bulge was visible again, there was also a second bulge on the upstream (leeward) face of the wavelet. The second bulge was caused by the low-speed fluid accumulation ahead of the crest. This makes a positive contribution to the $\overline{p' w'}$ correlation, i.e., it *extracts* energy from the wavelet.

The pressure–velocity correlation on the top streamline of the irrotational flow turns out to be negative, or order 50 $cm^3\ s^{-3}$, in the case of low steepness, but positive of order 100 $cm^3\ s^{-3}$ in the other cases (my estimates). The estimates arise from the difference between large positive and negative loops and are probably rather inaccurate. The only significant result is that these numbers are of the same order as estimated for the total energy supply to the water surface, and that they can be positive or negative, depending on the steepness of an individual wave.

In the case of the steeper waves, attenuating action of the low-speed fluid accumulation ("breaking," in a generalized sense) arises on account of upstream drainage of boundary layer fluid near the crest (in a wave-following frame), which occurs because the surface velocity exceeds the phase velocity in a stationary frame. A shear stress spike induces such surface flow long before the orbital velocity of the wave motion approaches the phase velocity: in the steeper wavelets of Okuda the velocity was only about $0.3c$ below the vortical layer, while it reached $1.2c$ or so at the surface. Figure 9 above already showed this.

It is legitimate to conclude that wavelets of such geometry that they cause shear stress spikes to occur near their crest grow while they are of suitably low steepness. As they become steeper, however, a feedback mechanism comes into play arresting further growth. The feedback mechanism consists of low-speed fluid accumulation ahead of the crest, made possible by the shear stress spike and associated upstream flow. When enough fluid accumulates ahead of the wave crest, the net $\overline{p'w'}$ correlation acting on the irrotational wave motion becomes positive and attenuates the wave. The attenuation occurs at a much smaller steepness than required for wave breaking in the absence of wind. (This result of the shear stress spike at a wave crest is akin to the effect of underlying long waves on the breaking of short waves, discussed by Phillips and Banner, 1974).

The wavelets observed by Okuda were very nearly in statistical equilibrium, i.e., neither their average wavelength nor their waveheight changed perceptibly with fetch, not at least at a rate for the temporal wave-energy change to be comparable to $\overline{\tau' u_0'}$. One concludes then, that although these wavelets were coupled to the wind in the sense of receiving a large energy input, they were able to dissipate that energy, principally by forming accumulations of fluid ahead of the wave crests, which moved with the waves. The question arises, under what conditions such statistical equilibrium is possible, or what constraints dissipation mechanisms place on the coupling of wind to wavelets.

7. Energy dissipation in the surface shear layer

Potentially important dissipation mechanisms in a turbulent surface shear layer are direct viscous dissipation by the mean flow, generation of short capillary waves (ripples), followed by viscous dissipation in the ripples, and a turbulent energy cascade ending also in viscous dissipation, but beginning with energy supply to larger eddies of the surface shear layer.

Of the three, the turbulent energy cascade at once appears to be the dominant mechanism. Okuda (1982a) points out that about 40% of the wavelets observed are characterized "by the occurrence of some systematic, rather persistent downward intrusion of water elements just leeward of the crest." A tongue of measurable vorticity extends in some such cases into the irrotational flow below. Earlier evidence of such "forced convection" on the leeward face of wind waves was presented by Toba *et al.* (1975). By contrast, direct viscous dissipation can readily be shown to be small compared to $\overline{\tau' u_0'}$, from direct observation of the surface shear layer. Estimation of energy dissipation by capillary waves is not so straightforward and is discussed briefly in the Appendix. The discussion again shows the area-average rate of energy supply to capillaries to be much less than $\overline{\tau' u_0'}$.

On account of their statistical equilibrium, the nearly irrotational wavelets no longer enter the problem of area-average energy balance. Further argument is therefore best conducted in a stationary coordinate frame. Supposing statistically steady conditions, the area-average balance equation for turbulent energy in the surface shear layer is written:

$$\tau \frac{\partial U}{\partial z} - \frac{\partial F}{\partial z} - \epsilon = 0 \tag{6}$$

with $U(z)$ the mean velocity, $F(z)$ vertical (upward) energy flux and $\epsilon(z)$ energy dissipation rate. The surface boundary condition is

$$-F = \overline{\tau' u_0'} - \overline{p' w_0'} \equiv F_0', \quad z = 0 \tag{7}$$

the mean stress velocity product being accounted for in the mean-flow energy equation (not discussed here).

In order to make Eq. (6) tractable it is necessary to introduce standard hypotheses regarding the properties of turbulence. Let the surface rate of energy dissipation and rms velocity be ϵ_0 and q_0. A dissipation length scale may be defined by

$$l_d = \frac{{q_0}^3}{\epsilon_0}. \tag{8}$$

It is realistic to suppose that q_0, l_d are the scales of energy-containing eddies in a surface sublayer that is strongly influenced by the direct energy input F_0'. As in other turbulent flows, these two scales will be supposed to determine all bulk properties of turbulence, including especially turbulent transport and dissipation. Thus the surface values of an eddy exchange coefficient ν_T and of a reciprocal decay time scale Λ, will be written:

$$\left.\begin{aligned} \nu_{T0} &= \frac{q_0 l_d}{R} \\ \Lambda_0 &= \frac{q_0}{l_d} \end{aligned}\right\} \tag{9}$$

with R an eddy Reynolds number.

A solution is sought for Eq. (6) valid for that portion of the surface shear layer in which the influence of the surface energy input is important, a kind of surface-stirred sublayer. Expecting the depth of this sublayer to be small, the stress will be supposed constant, $\tau = u_*^2$, as will the eddy viscosity and decay time scale (Eq. 9).

For the Reynolds stress, the energy flux, and the energy dissipation, the following simple closure formulae will be adopted:

$$\left.\begin{aligned} \tau &= \nu_T \frac{\partial U}{\partial z} \\ \epsilon &= \Lambda\left(\frac{1}{2} q^2\right) \\ F &= -\nu_T\left(\frac{1}{2}\frac{\partial q^2}{\partial z}\right) \end{aligned}\right\}. \tag{10}$$

The second of these relationships requires comment. In homogeneous turbulence, energy dissipation is usually set proportional to q^3/l_d, where q is the slowly decaying magnitude of rms velocity. In shear flow, where q varies rapidly in the cross-flow direction, dissipation changes are more nearly proportional to q^2 than to q^3, as several prototype examples discussed by Townsend (1956) show (for a detailed discussion of the example of the mixing layer see Csanady, 1963). The physical interpretation is that Λ is a characteristic of the large eddies of the flow, and is nearly constant across a shear layer. For the results that follow, the difference between this postulate and the conventional assumption of $\epsilon = q^3/l_d$, with q the *local*, rapidly varying value of rms velocity, is not very important, although the calculations are simpler with Eq. (10).

Substitution of Eq. (10) into (6) now results in a linear equation for the turbulent energy:

$$\nu_{T0}\frac{\partial^2 q^2}{\partial z^2} - \Lambda q^2 = -\frac{2u_*^4}{\nu_{T0}} \tag{11}$$

with the boundary condition

$$\frac{1}{2}\frac{\partial q^2}{\partial z} = \frac{F_0'}{\nu_{T0}}, \quad z = 0. \tag{12}$$

The solution satisfying the boundary condition and remaining finite at depth is:

$$\frac{1}{2} q^2 = \frac{u_*^4}{\nu_{T0}\Lambda} + \frac{F_0'}{(\nu_{T0}\Lambda)^{1/2}} e^{z/l_z} \tag{13}$$

where $l_z^2 = \nu_{T0}/\Lambda$. The extra energy of the turbulent motion due to the surface energy flux vanishes at depths much greater than l_z, so that l_z is a measure of the thickness of the stirred sublayer within which surface energy input is important. For vanishing F_0', the turbulent energy is constant with depth and should be equal to the energy in a classical constant stress layer for consistency. The constant term contains only one turbulence parameter, which is from Eq. (9):

$$\nu_{T0}\Lambda_0 = \frac{q_0^2}{R}. \tag{14}$$

Hence at vanishing F_0' the surface turbulence intensity is

$$q_0^2 = (2R)^{1/2} u_*^2, \quad F_0' \to 0. \tag{15}$$

According to data of Laufer, quoted by Townsend (1956), in a constant stress layer q_0^2 is about $8u_*^2$. Matching the result to this number requires $R = 32$, a value in the usual range of eddy Reynolds numbers.

With significant surface energy flux, the surface value of the turbulent intensity is, from (13) and (14)

$$q_0^2 = \frac{2Ru_*^4}{q_0^2} + \frac{2R^{1/2}F_0'}{q_0}. \tag{16}$$

To estimate the contribution due to the energy flux from this equation F_0' must be known. If the force of the wind is exerted predominantly by shear stress spikes over a field of short-crested wavelets of essentially similar geometry, F_0' should be nearly equal to $\overline{\tau' u_0'}$, and the peak of τ' should vary as u_*^2. The laboratory evidence also shows that the surface velocity at the crest is close to the phase velocity c—neither much smaller nor much larger for equilibrium conditions—presumably because otherwise the rate of fluid accumulation ahead of the crest would be either too slow or too fast for statistical balance between wave growth and attenuation. The stress–surface velocity correlation may therefore be taken to vary as wind stress times phase velocity:

$$\overline{\tau' u_0'} = \alpha u_*^2 c \approx F_0' \tag{17}$$

where the constant α may be estimated to be about 0.8 for the steeper wind-waves, on the basis of Okuda's laboratory observations, and somewhat less on an area-average basis, say $\alpha = 0.5$.

An independent estimate of the energy flux-related contribution to q_0^2 follows from the observed characteristics of the turbulent motion near the surface. The energy input was earlier seen to be manifested in the first instance by the appearance of isolated parcels of fluid of a velocity proportional to the celerity c of the wavelets. These occupy a certain small fraction of the surface and contribute on an area-average basis to q_0^2 the amount:

$$\Delta q_0^2 = \gamma c^2 \tag{18}$$

where γ is of the order of the area-fraction occupied by the parcels of fluid spilling over the windward face of wavelets. Putting this equal to the second term on the right of (16) one finds for q_0:

$$q_0 = \frac{2R^{1/2}\alpha u_*^2}{\gamma c}. \tag{19}$$

The surface turbulent intensity may now be eliminated from (16) and a relationship between c and u_* found:

$$\frac{c}{u_*} \approx \left(\frac{2\alpha R^{1/2}}{\gamma^{3/2}}\right)^{1/2} \equiv m \tag{20}$$

where advantage was taken of the fact that $\gamma \ll 1$.

If γ remains constant with changing u_* (as well as α and R), m = constant, and a simple linear relationship between c and u_* results. It is more likely, perhaps, that γ increases somewhat with u_* so that c increases less than in direct proportion to u_*. The general result of the above calculation is that c and u_* are related, on account of the energy balance of surface-layer turbulence, and the manner in which the surface values of turbulent velocity and length scale are set by the method of energy input. In other words, the statistical equilibrium of wavelets, in which intermittent wave growth is balanced, on the average, by attenuation, is only possible at a specific celerity, and hence wavelength. Earlier it was seen that the coincidence of shear stress spikes with wave crests, which couples such wavelets to the wind, requires a specific wave geometry (i.e., steepness, for constant l/k). Given coupling to the wind, however, constant steepness (on the average) can only be maintained if wave attenuation balances growth. Hence the coupled wavelets have not only a specific steepness, but also a specific wavelength.

As was already pointed out above, in the Tohoku University observations the wind wavelets, although irregular, had a clear dominant wavelength of around 12 cm (see Fig. 7). The same is true of the laboratory observations of Chang *et al.* (1971), carried out over wavelets about 27 cm long. However, the few observations of Okuda at a higher wind speed (u_* = 1.6 cm s^{-1}) do not support Eq. (20) with m = const, nor does the comparison of the Okuda and Chang *et al.* experiments, the celerity of the dominant wavelets increasing more slowly with u_* than a linear relationship would require. The question of the wind stress dependence of dominant wavelets coupled to the wind has not been examined systematically, however, and the significance of the departures from the linear relationship is not clear.

8. Dominant wind-wavelets and aerodynamic roughness

Some empirically determined properties of the turbulent flow on both sides of the air–sea interface provide qualified support for the conceptual model deduced above from laboratory evidence. This is true of the aerodynamic roughness of the sea surface, and of the surface velocity gradient just below the surface. The interpretation of the field evidence on these properties of the air–water interface in terms of the model rests, of course, on the assumption that the physical processes discovered in the laboratory also operate in the presence of longer waves, under the chaotic conditions characteristic of a natural wind-blown surface.

The approximate relationship (20) with the classical formula for the celerity of gravity waves gives the wavelength of the dominant wind-wavelets:

$$\lambda = 2\pi m^2 \frac{u_*^2}{g}. \tag{21}$$

The steepness $s = H/\lambda$ of the wavelets, measured by the waveheight-to-wavelength ratio, was earlier seen to be approximately constant ($s \approx 0.08$); hence their height is

$$H = 2\pi s m^2 \frac{u_*^2}{g} \equiv 2\pi s m^2 \frac{\rho_a}{\rho_w}\frac{u_{*a}^2}{g} \tag{22}$$

where ρ_a/ρ_w is the density ratio of air to water and u_{*a} is friction velocity in air. This result agrees in form with Charnock's (1955) postulate for the roughness parameter z_{0a} of the sea surface:

$$z_{0a} = a^{-1}\frac{u_{*a}^2}{g} \tag{23}$$

with $a \approx 80$. Wu (1969) has examined a large dataset and concluded that Eq. (23) applies approximately within a limited wind speed range, with $a \approx 90$. At low wind speeds ($u_* < 1$ cm s^{-1}) the formula overestimates roughness, the sea surface being under certain conditions even "supersmooth" (Csanady, 1974; Hsu and Hsu, 1983), while in very strong winds ($u_* > 2.5$ cm s^{-1}) the roughness increases faster than Eq. (23) predicts. These observed facts are consistent with the notion that the postulates on which the energy balance is based break down in very light or very strong winds. In very light winds it is impossible to satisfy Eq. (20), because the phase velocity of short wavelets has a minimum at c = 23 cm s^{-1}. Turbulent energy dissipation according to the above hypotheses cannot be sustained in such light winds and wavelets cannot acquire the steepness which they exhibit in stronger winds. On the other hand, in very strong winds the disruption of the sea surface by foam and spray presumably becomes significant.

The ratio H to z_{0a} is, from (22) and (23):

$$\frac{H}{z_{0a}} = 2\pi s a m^2 \frac{\rho_a}{\rho_w}. \tag{24}$$

Okuda's laboratory data suggest the value m = 50 for the constant in Eq. (20). Using a = 90, s = 0.08, ρ_w/ρ_a = 800 one calculates $H/z_{0a} \approx 140$, which is rather larger than the ratio of sand-grain diameter to roughness length in the classical Nikuradse (1933) experiments, $d/z_{0a} \approx 30$. Lettau (1969) has discussed variations of h^*/z_{0a} for different types of roughness, with h^* the maximum height of roughness. Most conclusive

were the experiments using bushel baskets as roughness elements on the frozen surface of Lake Mendota: unless the baskets were spaced very closely, the roughness parameter increased in direct proportion to their density on the ice. This was true for the range $h^*/z_{0a} = 20$ to 2000. In the above analysis, the parameter γ is mostly a measure of the area density of the high-speed parcels of fluid, which is proportional to the area-density of the steeper wavelets acting as roughness elements. When Eq. (20) is substituted into (24), it shows z_{0a} to be proportional to $\gamma^{3/2}$, suggesting an even greater influence of roughness element density on z_{0a} than in the case of solid objects placed on a flat surface. The quantitative result, $H/z_{0a} \approx 140$ is roughly consistent with Lettau's empirical ratios for bushel baskets if γ is of order 0.01. From Eq. (20), with $m = 50$, $\alpha = 0.5$ and $R = 32$ one finds $\gamma = 0.017$.

9. Surface shear layer and water-side roughness

The gradient of the mean velocity at the surface is by the definition of the eddy viscosity:

$$\frac{dU}{dz} = \frac{u_*^2}{\nu_{T0}}. \tag{25}$$

From Eqs. (9) and (19) one finds

$$\frac{dU}{dz} = \frac{\gamma R^{1/2}}{2\alpha} \cdot \frac{c}{l_d}. \tag{26}$$

To proceed further, it is necessary to introduce an Ansatz for the length scale l_d. The manner in which surface turbulence is produced (formation of fluid accumulations traveling with wave crests) suggests:

$$l_d = \beta\lambda \tag{27}$$

where β is presumably of order one. Substituting into (26) and using again the classical formula for the wavelength of gravity waves one finds with the aid of Eq. (20):

$$\frac{dU}{dz} = n\frac{g}{u_*} \tag{28}$$

where

$$n = \frac{R^{1/4}\gamma^{7/4}}{2\pi(2\alpha)^{3/2}\beta}.$$

The result that the surface velocity gradient should *decrease* with increasing wind stress is counterintuitive, and provides a particularly useful check on the model. The only relevant evidence seems to have been reported by Churchill and Csanady (1983), who tabulated the velocity of a surface drifter (mean depth 0.012 m) relative to a drogue with a mean depth of 1.8 m, as obtained in a number of experiments on Cape Cod Bay and on Lake Huron. There are several complications in such observations, and the velocity difference between two fixed levels can only be used as an approximate measure of the surface velocity gradient at moderately high wind speeds, provided also that the direction of the surface shear (θ_s) coincides with the direction of the wind (θ_w).

Figure 10 shows this velocity difference for all the reported observations with a 3-m wind greater than 3.5 m s^{-1}, and a directional departure ($\theta_s - \theta_w$) less than 15°, versus wind speed. A decrease of shear with increasing wind is indicated within a limited range of u_*. As pointed out before, the simple relationships are not expected to hold either at very low or at very high u_*.

The average of three well documented runs of observations carried out at $u_* \approx 1$ cm s^{-1} gave a value for the surface velocity gradient of 0.813 s^{-1}. Substituting into Eq. (28) this yields $n = 0.83 \times 10^{-3}$. The definition of n, with the previous estimates $R = 32$, $\gamma = 0.017$, $\alpha = 0.5$ implies now

$$\beta = 0.365.$$

With all the nondimensional parameters having been assigned rough values, the various sublayer characteristics can be estimated from earlier results: $q_0 \approx 6.7$ cm s^{-1}, $l_d = 6$ cm, $\nu_T = 1.2$ cm^2 s^{-1} (this follows directly from u_* and dU/dz). $\Lambda = 1.2$ s^{-1}, $l_z = 1.0$ cm. The last estimate verifies *a posteriori* the hypothesis that the sublayer, influenced by the surface energy input, is thin.

At increasing depth, the sublayer merges into a constant-stress layer with a logarithmic velocity profile, characterized by a relatively large roughness length. This was attributed to surface turbulence associated with breaking wavelets (Csanady, 1984); the discussion above has elucidated some details. A quantitative estimate for the waterside hydrodynamic roughness can be found by a simple approximate theory as follows:

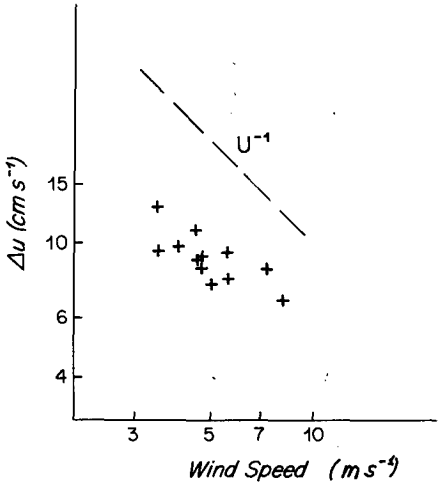

FIG. 10. Velocity difference between a surface drifter (mean depth 1.2 cm) and a near-surface drogue (mean depth 1.8 m) versus wind speed. Only those observations are shown in which the direction of surface shear coincides with wind direction (within 15°) and the wind speed is at least 3.5 m s^{-1}. From data tabulated by Churchill and Csanady (1983).

Let a sublayer characterized by constant eddy viscosity ν_T—as just used in the calculations—be matched to a classical constant stress layer, in which the eddy viscosity increases linearly with distance from the boundary:

$$\nu_T = \nu_{T0} = \text{const}, \quad |z| < z_m$$
$$\nu_T = \kappa u_* |z|, \quad |z| > z_m \tag{29}$$

where κ is Karman's constant and z_m is a matching depth. To ensure the continuity of the velocity gradient this depth has to be

$$z_m = \frac{\nu_{T0}}{\kappa u_*}. \tag{29a}$$

The velocity distributions above and below the matching depth are

$$\left.\begin{aligned} U &= U_s + \frac{u_*^2}{\nu_T} z \\ U &= U_s - \frac{u_*}{\kappa} \ln \frac{|z|}{z_0} \end{aligned}\right\} \tag{30}$$

where U_s is the surface velocity. These are continuous if

$$\ln \frac{z_m}{z_0} = 1 \tag{31}$$

which is equivalent to

$$z_0 = \frac{\nu_{T0}}{e\kappa u_*}. \tag{32}$$

Equation (9) and some subsequent results imply now that z_0 is proportional to l_d or λ or waveheight H. A quantitative estimate from the last equation for $u_* = 1$ cm s^{-1} is

$$z_0 = 1.1 \text{ cm} \quad (u_* = 1 \text{ cm s}^{-1})$$

with $\nu_{T0} = 1.2$ cm^2 s^{-1}, derived from the observations.

The observations yielded an average roughness, extracted from a number of velocity profiles, of

$$z_0 = \frac{22}{30} \frac{\nu_{T0}}{u_*} = 0.83 \text{ cm}.$$

It is seen that the simple matching theory gives a close approximation. Upon substituting Eq. (9) and later results into Eq. (32) one finds

$$z_0 = \frac{(2\alpha)^{1/2}}{\kappa e R^{3/4} \gamma^{1/4}} l_d \approx 0.19 l_d \equiv 0.07\lambda. \tag{33}$$

This depends only weakly on the area ratio of high-speed fluid parcels γ so that z_0 presumably tracks l_d, and the wavelength λ of the dominant waves, fairly closely. The immediate reason why z_0 is so much larger on the water than on the air side is that ν_{T0} is large. This is due in turn to the high value of q_0, which arises from the direct energy input to turbulence by the wind, and from the relatively large length scale.

With all the uncertainties of the observational evidence, the conclusions one draws from the analysis of the turbulent energy balance give a consistent picture of the structure of the free-surface shear layer. The estimated quantitative parameters, γ, R, etc. are crude, but their magnitude is physically reasonable.

10. Concluding remarks

The laboratory evidence showed that certain wavelets become coupled to the wind, in the sense of receiving significant energy input from the air flow, and yet retaining, on the average, the same steepness and amplitude. The physical processes that make this possible—air flow separation and reattachment, formation of fluid accumulation ahead of wave crests, etc.—are all of a small spatial scale. On a natural wind-blown surface some complicating factors are present, notably much longer waves of large amplitude, and may affect the smaller-scale processes to some degree. It is difficult to see, however, how the long waves could make wind–wavelet coupling of the kind seen in the laboratory impossible. There is direct evidence to show that short-crested wavelets in the same wavelength range as studied in the laboratory are present on the sea surface, and that their spectral intensity increases in some manner with u_*. For some time it has been widely accepted that short waves transfer momentum to the surface shear flow in water. It is certainly plausible to take the further step of supposing that the transfer mechanism is, in its essentials, revealed by the laboratory investigations, whatever the modifications attributed to long waves. Field evidence surveyed in the last two sections supports this hypothesis, but of course specific field studies are needed to verify the details.

As a final note, it should be mentioned that the relationship $c \sim u_*$ was conjectured or derived from heuristic arguments relating to the *air* flow alone by Wu (1970) and Melville (1977). Based on the arguments of Banner and Melville (1976), Melville (1977) also postulates a connection between wave breaking and air flow separation, and he supposes further that the force of the wind is exerted by means of form drag. As discussed here in detail, these hypotheses are at variance with observational evidence. The arguments advanced in the present paper are entirely different, in that the $c \sim u_*$ relationship is derived from the turbulent energy balance below the surface, although the characteristics of separating air flow are taken to be such as to maintain a specific kind of wavelet in statistical equilibrium. The important point is perhaps that, in order to understand the mechanism of momentum transfer from air to water, it is necessary to consider *both* the air side and the water side: arguments relating to air flow alone, or to the wave motion alone, must necessarily remain inconclusive.

Acknowledgements. The work described in this paper is part of a study of the dynamics of centimetric waves

in the ocean, carried out in collaboration with M. H. Freilich of the Jet Propulsion Laboratory and supported by NASA, Oceanic Processes Branch. I have benefited from many discussions with and comments by Mike Freilich. I. S. F. Jones also kindly sent me some useful comments.

APPENDIX

Energy Dissipation by Capillary Waves

A somewhat exotic pathway to viscous energy dissipation is the generation of capillaries at the wave crest, their leeward propagation, and eventual dissipation. The phenomenon has been discussed by Munk (1955) and Longuet-Higgins (1963). Relevant theoretical results have been given also by Lamb (1932) and Crapper (1970).

The sharp-crested wavelets observed by Okuda show the characteristic forward-leaning asymmetry of waves near breaking. This is rather unlike the classical finite-amplitude underlying wave model used by Longuet-Higgins (1963) and also by Crapper (1970). Both authors emphasize the weakness of this model, and Chang *et al.* (1978) explicitly point out that the asymmetry of the observed waves makes them unlike any of the available finite amplitude models. The discrepancy is significant mainly in the neighborhood of the crest.

A plausible alternative model is to think of the asymmetric wave as containing a low-speed fluid accumulation at the crest, which is spilling over the forward face, much as envisaged by Longuet-Higgins and Turner (1974). At the toe of the spilling fluid the pressure on the underlying, supposedly irrotational flow streamline rises suddenly. A simple assumption is that the pressure rises instantly to some value p_s and remains constant afterwards. Lamb's (1932) model can then be applied, *mutatis mutandis,* with the derivative of the pressure being now a delta function, instead of the pressure itself, which is the basic assumption in Lamb's model.

This "spilling breaker" model yields the surface slope at the origin, transcribed from Lamb's Eq. (19):

$$\left.\frac{d\zeta}{dx}\right|_0 = \frac{p_s}{\pi T(\kappa_2 - \kappa_1)} \ln \frac{\kappa_2}{\kappa_1} \tag{A1}$$

where T is kinematic surface tension, and κ_1, κ_2 are wavenumbers of gravity and capillary waves respectively, at the phase velocity c of the wind wavelets. These are roots of the equation

$$T\kappa^2 - c^2\kappa + g = 0. \tag{A2}$$

The energy supply to the capillaries at the toe of the spilling fluid is $p_s w$, the vertical velocity w being c times the slope, hence:

$$E_c = p_s c \left.\frac{d\zeta}{dx}\right|_0 = \frac{{p_s}^2 c}{\pi T(\kappa_2 - \kappa_1)} \ln \frac{\kappa_2}{\kappa_1}. \tag{A3}$$

Energy transfer to capillaries is effective over a distance of order κ_2^{-1}, hence the wavelength-averaged energy supply rate is

$$\bar{E}_c = \frac{{p_s}^2 c \kappa_1}{\pi T \kappa_2(\kappa_2 - \kappa_1)} \ln \frac{\kappa_2}{\kappa_1}. \tag{A4}$$

At a phase speed of $c = 50$ cm s^{-1}, with $T = 72$ cm^3 s^{-2} (clean water) the two roots of Eq. (A2) are $\kappa_1 = 0.4$, $\kappa_2 = 34.3$ cm^{-1}. The pressure p_s is reasonably assumed the equivalent of a 1-mm layer of spilling fluid. This then yields $E_c \approx 10$ cm^3 s^{-3}. Because only a fraction of the surface contains spilling breakers, the area-average dissipation rate is again much less than $\overline{\tau' u_0'}$.

REFERENCES

Banner, M. L., and W. K. Melville, 1976: On the separation of air flow over water waves. *J. Fluid Mech.*, **77,** 825–842.

Battjes, J. A., and T. Sakai, 1981: Velocity field in a steady breaker. *J. Fluid Mech.*, **111,** 421–437.

Bradshaw, P., and F. Y. F. Wong, 1972: The reattachment and relaxation of a turbulent shear layer. *J. Fluid Mech.*, **52,** 113–135.

Brown, G. L., and A. S. W. Thomas, 1977: Large structure in a turbulent boundary layer. *Phys. Fluids,* **20,** S 243–252.

Castro, I. P., and A. G. Robbins, 1977: The flow around a surface-mounted cube in uniform and turbulent streams. *J. Fluid Mech.*, **79,** 307–335.

Chandrsuda, C., and P. Bradshaw, 1981: Turbulence structure of a reattaching mixing layer. *J. Fluid Mech.*, **110,** 171–194.

Chang, P. C., E. J. Plate and G. M. Hidy, 1971: Turbulent air flow over the dominant component of wind-generated water waves. *J. Fluid Mech.*, **47,** 183–208.

——, R. N. Wagner and H. C. Yuen, 1978: Measurement of high frequency capillary waves on steep gravity waves. *J. Fluid Mech.*, **86,** 401–413.

Charnock, H., 1955: Wind stress on a water surface. *Quart. J. Roy. Meteor. Soc.*, **81,** 639–640.

Churchill, J. H., and G. T. Csanady, 1983: Near-surface measurements of quasi-Lagrangian velocities in open water. *J. Phys. Oceanogr.*, **13,** 1669–1680.

Clauser, F. H., 1956: The turbulent boundary layer. *Adv. Appl. Mech.*, **4,** 1–56.

Crapper, G. D., 1970: Non-linear capillary waves generated by steep gravity waves. *J. Fluid Mech.*, **40,** 149–159.

Csanady, G. T., 1963: On the energy balance of a turbulent mixing layer. *J. Fluid Mech.*, **15,** 545–559.

——, 1974: The "roughness" of the sea surface in light winds. *J. Geophys. Res.*, **79,** 2747–2751.

——, 1984: The free surface turbulent shear layer. *J. Phys. Oceanogr.*, **14,** 402–411.

Gent, P. R., and P. A. Taylor, 1977: A note on "separation" over short wind waves. *Bound. Layer Meteor.*, **11,** 65–87.

Hsu, C. T., and E. Y. Hsu, 1983: On the structure of turbulent flow over a progressive water wave: theory and experiment in a transformed wave-following coordinate system. *J. Fluid Mech.*, **131,** 123–153.

Hunt, J. C. R., C. J. Abell, J. A. Peterka and H. Woo, 1978: Kinematical studies of the flows around free or surface-mounted obstacles; applying topology to flow visualization. *J. Fluid Mech.*, **86,** 179–200.

Jeffreys, H., 1925: On the formation of water waves by wind. *Proc. Roy. Soc. London* **A107,** 189–205.

Kawai, S., 1979: Generation of initial wavelets by instability of a coupled shear flow and their evolution to wind waves. *J. Fluid Mech.*, **93,** 661–703.

——, 1981: Visualization of airflow separation over wind-wave crests under moderate wind. *Bound. Layer Meteor.*, **21,** 93–104.

——, 1982: Structure of air flow separation over wind wave crests. *Bound. Layer Meteor.*, **23,** 503–521.

Lamb, H., 1932: *Hydrodynamics.* Cambridge University Press, 78 pp.

Laufer, J., 1975: New trends in experimental turbulence research. *Annual Reviews in Fluid Mechanics,* Vol. 1 Annual Reviews, 307–326.

Lettau, H., 1969: Note on aerodynamic roughness-parameter estimation on the basis of roughness-element description. *J. Appl. Meteor.*, **8,** 828–832.

Lighthill, M. J., 1963: Boundary layer theory. *Laminar Boundary Layers,* L. Rosenhead, Ed., Oxford University Press, 46–113.

Longuet-Higgins, M. S., 1963: The generation of capillary waves by steep gravity waves. *J. Fluid Mech.*, **16,** 138–159.

——, 1969a: A nonlinear mechanism for the generation of sea waves. *Proc. Roy. Soc. London* **A31,** 192–198.

——, 1969b: Action of a variable stress at the surface of water waves. *Phys. Fluids,* **12,** 737–740.

——, and J. S. Turner, 1974: An 'entraining plume' model of a spilling breaker. *J. Fluid Mech.*, **83,** 1–20.

McLean, J. W., 1982: Instabilities of finite amplitude water waves. *J. Fluid Mech.*, **114,** 315–330.

Meiron, D. I., P. G. Saffman and H. C. Yuen, 1982: Calculation of steady three-dimensional deep-water waves. *J. Fluid Mech.*, **124,** 109–121.

Melville, W. K., 1977: Wind stress and roughness length over breaking waves. *J. Phys. Oceanogr.*, **7,** 702–710.

Munk, W. H., 1955: High frequency spectrum of ocean waves. *J. Mar. Res.*, **14,** 302–314.

Nikuradse, J., 1933: Strömungsgesetze in rauhen Rohren. *VDI Forschungsheft 361.*

Okuda, K., 1982a: Internal flow structure of short wind waves, Part I. On the internal vorticity structure. *J. Oceanogr. Soc. Japan,* **38,** 28–42.

——, 1982b: Internal flow structure of short wind waves. Part II. The streamline pattern. *J. Oceanogr. Soc. Japan,* **38,** 313–322.

——, 1982c: Internal flow structure of short wind waves. Part III, Pressure distributions. *J. Oceanogr. Soc. Japan,* **38,** 331–338.

——, S. Kawai, M. Tokuda and Y. Toba, 1976: Detailed observation of the wind-exerted surface flow by use of flow visualization methods. *J. Oceanogr. Soc. Japan,* **32,** 53–64.

——, —— and Y. Toba, 1977: Measurement of skin friction distribution along the surface of wind waves. *J. Oceanogr. Soc. Japan,* **33,** 190–198.

Peregrine, D. H., and I. A. Svendsen, 1979: Spilling breakers, bores and hydraulic jumps. *Proc. 16th Coastal Engineering Conf., Vol. I,* New York, Amer. Soc. Civil Engineers, 540–550.

Phillips, O. M., and M. L. Banner, 1974: Wave breaking in the presence of wind drift and swell. *J. Fluid Mech.*, **66,** 625–640.

Roll, H. U., 1965: *Physics of the Marine Atmosphere.* Academic Press, 426 pp.

Schooley, A. H., 1963: Simple tools for measuring wind fields above wind-generated water waves. *J. Geophys. Res.*, **68,** 5497–5504.

Stewart, R. W., 1961: The wave drag of wind over water. *J. Fluid Mech.*, **10,** 189–194.

——, 1974: The air–sea momentum exchange. *Bound. Layer Meteor.*, **6,** 151–167.

Su, M. Y., 1982: Three-dimensional deep-water waves. Part I, Experimental measurement of skew and symmetric wave patterns. *J. Fluid Mech.*, **124,** 73–108.

——, M. Bergin, P. Marler and R. Myrick, 1982: Experiments on nonlinear instabilities and evolution of steep gravity-wave trains. *J. Fluid Mech.*, **124,** 45–72.

Thomas, A. S. W., and M. K. Bull, 1983: On the role of wall-pressure fluctuations in deterministic motions in the turbulent boundary layer. *J. Fluid Mech.*, **128,** 283–322.

Toba, Y., M. Tokuda, K. Okuda and S. Kawai, 1975: Forced convection accompanying wind waves. *J. Oceanogr. Soc. Japan,* **31,** 192–198.

Townsend, A. A., 1956: *The Structure of Turbulent Shear Flow.* Cambridge University Press, 315 pp.

Ursell, F., 1956: Wave generation by wind. *Surveys in Mechanics,* C. K. Batchelor and R. M. Davies, Eds., Cambridge University Press, 216–249.

Willmarth, W. W., 1975: Structure of turbulence in boundary layers. *Adv. Appl. Mech.*, **15,** 159–254.

Wu, J., 1969: Wind stress and surface roughness at air–sea interface. *J. Geophys. Res.*, **74,** 444–455.